2018

Ion selective separators based on graphene oxide for stabilizing lithium organic batteries

Yuede Pan
Chinese Academy of Sciences, University of Wollongong, yp388@uowmail.edu.au

Junran Hao
Chinese Academy of Sciences, Beihang University

Xuanbo Zhu
Chinese Academy of Sciences

Yahong Zhou
Chinese Academy of Sciences

Shulei Chou
University of Wollongong, shulei@uow.edu.au

Publication Details

Pan, Y., Hao, J., Zhu, X., Zhou, Y. & Chou, S. (2018). Ion selective separators based on graphene oxide for stabilizing lithium organic batteries. Inorganic Chemistry Frontiers, 5 (8), 1869-1875.

Ion selective separators based on graphene oxide for stabilizing lithium organic batteries

Abstract
Ion selective membranes exist widely in the biological world and have been mimicked by scientists and engineers for the purpose of manipulating ion flow. For instance, polymers with sulfonate groups like Nafion are applied in proton exchange membrane fuel cells for facilitating proton transport whilst blocking other species. Herein, ion selective separators composed of graphene oxide (GO) and Super P (or graphene) are applied for stabilizing lithium organic batteries. The reconstructed GO sheets form numerous negatively charged nanochannels, which selectively allow the transport of lithium ions and reject the electroactive organic anions. Meanwhile, Super P (or graphene) on top of the coating layer functions as the upper current collector for reactivating the electroactive organic species. In this work, two typical carbonyl electrode materials with, respectively, two (anthraquinone, AQ) and four (perylene-3,4,9,10-tetracarboxylic dianhydride, PTCDA) carbonyl groups are applied as examples. Compared to the pristine Celgard separator, the ion selective separators enable significantly alleviated self-discharge, improved coulombic efficiency and cycling stability.

Disciplines
Engineering | Physical Sciences and Mathematics

Publication Details
Pan, Y., Hao, J., Zhu, X., Zhou, Y. & Chou, S. (2018). Ion selective separators based on graphene oxide for stabilizing lithium organic batteries. Inorganic Chemistry Frontiers, 5 (8), 1869-1875.

INORGANIC CHEMISTRY
FRONTIERS

RESEARCH ARTICLE

View Article Online
View Journal | View Issue

Cite this: *Inorg. Chem. Front.*, 2018, **5**, 1869

Ion selective separators based on graphene oxide for stabilizing lithium organic batteries

Yuede Pan, †[a,b] Junran Hao,[a,c] Xuanbo Zhu,[a] Yahong Zhou *[a] and Shu-Lei Chou *[b]

Received 20th April 2018,
Accepted 18th May 2018

DOI: 10.1039/c8qi00374b

rsc.li/frontiers-inorganic

Ion selective membranes exist widely in the biological world and have been mimicked by scientists and engineers for the purpose of manipulating ion flow. For instance, polymers with sulfonate groups like Nafion are applied in proton exchange membrane fuel cells for facilitating proton transport whilst blocking other species. Herein, ion selective separators composed of graphene oxide (GO) and Super P (or graphene) are applied for stabilizing lithium organic batteries. The reconstructed GO sheets form numerous negatively charged nanochannels, which selectively allow the transport of lithium ions and reject the electroactive organic anions. Meanwhile, Super P (or graphene) on top of the coating layer functions as the upper current collector for reactivating the electroactive organic species. In this work, two typical carbonyl electrode materials with, respectively, two (anthraquinone, AQ) and four (perylene-3,4,9,10-tetracarboxylic dianhydride, PTCDA) carbonyl groups are applied as examples. Compared to the pristine Celgard separator, the ion selective separators enable significantly alleviated self-discharge, improved coulombic efficiency and cycling stability.

Introduction

The separator in a battery system plays an important role in physically and electronically separating the cathode and the anode to prevent a short circuit, meanwhile allowing wetting by the electrolyte and the transport of lithium ions between the electrodes.[1–6] The separator is a key component to make rechargeable batteries function as energy storage systems, transforming chemical energy into electric energy at discharge, and *vice versa* at charge. Besides these fundamental roles, the separator can be endowed with additional serviceable functions by applying new configurations or materials, in order to overcome some specific practical problems. For example, to improve safety and endurance, commercial polymer separators can be coated by ceramic particles (*e.g.*, nanosized Al_2O_3 powder).[7]

Another important function of battery separators can be ion selectivity. Ion selective separators are indispensable components for fuel cells and redox flow batteries.[8–10] Otherwise, the unwanted transport of certain charged species can cause the defunctionalisation of these battery types. For instance, vanadium redox flow batteries utilize Nafion as the separator, which prevents the crossover of vanadium ions. For lithium batteries, ion selective separators have recently been applied to manipulate ion transport through the separator. As summarized in our recent review paper, ion selective separators are studied mainly in lithium battery systems with cathode materials of sulphur, oxygen and organic molecules.[6] In lithium sulphur batteries, the polysulfide shuttling problem can be eliminated by utilizing ion selective separators to block the electronegative polysulfide ions. The reported materials include Nafion,[11,12] graphene oxide[13] and a Nafion/graphene oxide composite.[14] Both Nafion and graphene oxide have negatively charged nanopores, which allow the transport of lithium ions and block polysulfide anions. In lithium air batteries, preventing moisture from permeating to the anode side can be achieved by employing ion selective separators like superior lithium ion conductors.[15]

Like the battery systems mentioned above, lithium organic batteries are also plagued by the unwanted diffusion issue and ion selective separators can be an effective solution. In lithium organic batteries, the organic cathode molecules and their corresponding discharge products and intermediates tend to easily dissolve in the liquid electrolyte, causing problems including serious self-discharge, low coulombic efficiency (CE), and quick capacity decay.[16,17] This high solubility of

[a]*Laboratory of Bioinspired Smart Interfacial Science, Technical Institute of Physics and Chemistry, Chinese Academy of Sciences, Beijing 100190, China. E-mail: zhouyh@mail.ipc.ac.cn*
[b]*Institute for Superconducting and Electronic Materials, University of Wollongong, New South Wales, 2522, Australia. E-mail: shulei@uow.edu.au*
[c]*Key Laboratory of Bio-inspired Smart Interfacial Science and Technology of the Ministry of Education, School of Chemistry, Beihang University, Beijing 100191, China*
† Dr Y. Pan now works as an engineer in the Fundamental R&D Department at Zhuhai Coslight Battery Co., Ltd.

small organic molecules in an aprotic solvent has been taken as an advantage to produce catholytes and anolytes for organic redox flow batteries.[9] In lithium organic batteries, the electroactive organic species can dissolve in the electrolyte, accumulate and become inactive at the cathode/separator interface and inside the micropores of the separator. The electroactive species also migrate to the lithium anode to form an unstable solid electrolyte interface on the anode surface. This irreversible loss of the electroactive species results in poor battery performances.[18–21] Song *et al.* prepared an ion selective separator based on Nafion and successfully attained high performance for the organic cathode of 1,1′-iminodianthraquinone.[22] However, reports on introducing the ion selective separator into lithium organic batteries have been rare.

Herein, we demonstrate a thin bicomponent layer constructed on a Celgard separator for application in lithium organic batteries. The bicomponent layer consists of graphene oxide (GO) and Super P (or graphene). The reconstructed GO sheets form numerous negatively charged nanochannels, which selectively facilitate the transport of counter-ions (*e.g.*, lithium ions) and reject co-ions (*e.g.*, the electroactive organic anions). The negative charge of the nanochannels originates from the carboxylic acid and phenolic hydroxyl groups on the GO sheets. Super P (or graphene) functions as the upper current collector for the organic cathode to improve active material utilization.[20,23] This bicomponent structure integrates the dual functions of ion selectivity from GO and an upper current collector from Super P (or graphene).

Taking carbonyl organic cathode materials as an example, particularly for smaller molecules, all the organic molecules, the discharge products and intermediates are soluble in the electrolyte (Fig. 1a). With the application of the bicomponent layer coated separator, the electroactive species are prevented from diffusing to the anode side and their utilization is significantly improved (Fig. 1b). Meanwhile, the contamination of the electroactive organic species towards the lithium anode is alleviated. The ion selective separator was prepared by a simple vacuum filtration method. A dispersion of GO and Super P (or graphene) was filtered using a Celgard separator as the filter paper (Fig. 1c). GO sheets were reconstructed to form numerous nanochannels with negative charge. The nanochannels selectively allow the transport of counter-ions and reject co-ions. Meanwhile, Super P (or graphene) acts as the upper current collector to provide reactivation sites for the dissolved electroactive species. With anthraquinone (AQ) and perylene-3,4,9,10-tetracarboxylic dianhydride (PTCDA) as two examples of organic cathode materials, it is demonstrated that the ion selective separator effectively stabilizes the open circuit voltage (OCV), significantly improves the CE and greatly enhances the cycling stability. For instance, with an ion selective separator, the capacity retention of the PTCDA cathode increases from 27% to 79% after 200 cycles and the CE improves from lower than 90% to above 99.5%, compared to that with a pristine Celgard separator.

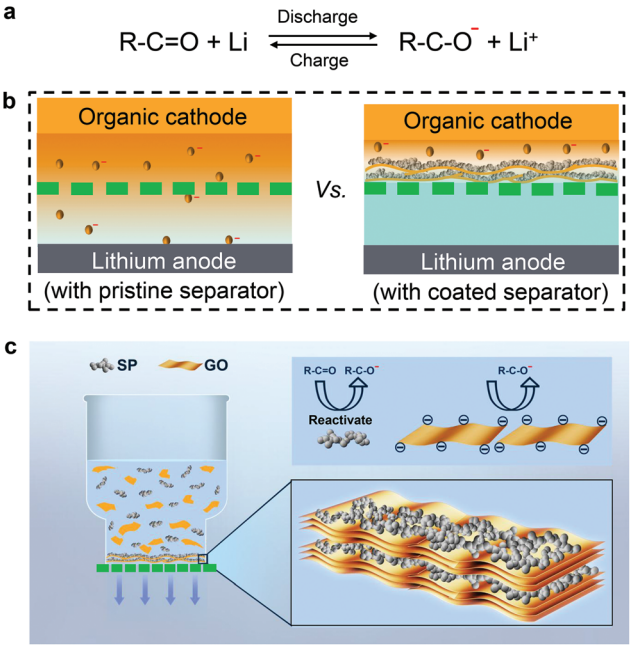

Fig. 1 Schematic illustrations of the application of the ion selective separator based on GO in lithium-organic batteries. (a) The electrochemical charge/discharge reactions of an electroactive organic molecule with conjugated carbonyl groups. (b) The blocking of the dissolved electroactive organic molecules and anions by the ion selective separator. (c) The preparation of the thin bicomponent layer coated separator and its functioning mechanism in a lithium-organic battery.

Experimental

Materials and characterization

Anthraquinone (AQ) and perylene-3,4,9,10-tetracarboxylic dianhydride (PTCDA) were purchased from J&K Chemical Co., Ltd. Graphene oxide (GO) and graphene were purchased from Nanjing XFNANO Co., Ltd. Celgard 2325 was purchased and used as the separator substrate. A mixture of GO and Super P (or graphene) was dispersed in deionized water (1 mg ml^{-1}) under sonication. The weight ratio between GO and Super P is 1 : 2 and that between GO and graphene is 1 : 1. 1 ml of the suspension was re-dispersed in ethanol (10 ml) and vacuum filtrated to yield a coating layer with an areal density of around 0.1 mg cm^{-2} on a pristine Celgard 2325 separator. Morphologies were observed using a field-emission scanning electron microscope (SEM, Hitachi S4800). Visual experiments were carried out using an H-type diffusion glass cell composed of two halves. The electrode was prepared by coating the slurry of AQ onto a nickel foam current collector. A constant potential of 2.2 V was applied with lithium as the counter electrode.

Battery assembly and test

AQ (or PTCDA) was mixed with Super P and a poly(vinylidene difluoride) (PVDF) binder with a weight ratio of 6 : 3 : 1 to form a homogeneous slurry, which was coated onto carbon-coated aluminum foil to form an organic cathode with an active material loading of 1.6 mg cm^{-2}. CR2032 coin cells were

assembled in an argon-filled glove box (H_2O < 0.1 ppm and O_2 < 0.1 ppm) by pairing the organic cathode and the lithium anode. The coating layer of the separators faces the organic cathode. The circular diameters of the organic cathode, the lithium foil and the separator were 12 mm, 14 mm, and 16 mm, respectively. The disassembling of coin cells was also conducted in the glove box. The electrolyte was 1.0 M lithium bis(trifluoromethanesulphonyl)imide (LiTFSI) in a binary mixture of 1,3-dioxolane (DOL) and 1,2-dimethoxyethane (DME) (v/v, 1 : 1). For each coin cell, 40 μl of the electrolyte was added. Galvanostatic charge/discharge was performed on a LAND battery testing machine (Wuhan, China) with a voltage window between 1.7 and 3.5 V. The specific capacities of the coin cells were calculated based on the weight of the active material of AQ or PTCDA. Cyclic voltammetry (CV) curves were recorded with a VSP-300 electrochemical workstation with a sweep rate of 0.1 mV s^{-1}.

Results and discussion

GO/Super P (GO/SP)-coated separators (denoted as GO/SP-P) and GO/graphene (GO/G)-coated separators (denoted as GO/SP-P or GO/G-P) were prepared by a vacuum filtration method. The GO/SP or GO/G mixture was first dispersed in deionized water to form a suspension. There is an electrostatic repulsion between the GO sheets with a high negative charge at the surface. The negative charge originates from the carboxylic acid and phenolic hydroxyl groups on the GO sheets. The zeta potential of GO was determined to be −34 mV, lower than −30 mV, indicating that the mutual repulsion between the GO nanosheets is strong enough to produce a stable dispersion.[24] In contrast, the SP or G particles easily precipitate in water due to their low surface charge densities (zeta potential of 9 and −11 mV, respectively).

The structures of the Celgard separator (denoted as pristine P) and the coated bicomponent layer were characterized by SEM (Fig. 2). Pristine P is composed of three layers with PE sandwiched between two outer layers of PP, with a total thickness of 25.8 μm and each layer of PP or PE possessing a similar thickness of 8–9 μm (Fig. 2a). The top-view SEM image presents the microporous structure of the separator (Fig. 2b). The coated bicomponent GO/SP layer shows SP particles between and on top of the crumpled GO films, with a total thickness of 905 nm (Fig. 2c). The reconstructed GO sheets possess numerous negatively charged nanochannels; both the thickness of the GO sheets and the dimension of the thus-formed nanochannels are approximately 1 nm.[25,26] The negatively charged nanochannels selectively allow the transport of lithium ions and reject the electroactive organic anions.[27] An examination of the top-view image indicates that on top of the bicomponent layer there are scattered SP particles (Fig. 2d), which would have an intimate contact with the organic cathode, acting as an upper current collector. The cross-sectional and top-view SEM images of the GO/G bicomponent layer can be seen in Fig. 2e and f, respectively. The thickness of the GO/G coating layer is around 1.4 μm. The surface of the GO/G bicomponent layer is crumpled, owing to the overlapping of the GO nanosheets and the G nanosheets, both of which have similar dimensions of several hundred nanometers. Similar to GO/SP, the electronic conductivity of G and the cation selectivity of the layered GO nanosheets are expected to synergistically improve the active material utilization and the cycling stability.

To characterize the coated separators, two typical carbonyl organic molecules, *i.e.*, anthraquinone (AQ) and perylene-3,4,9,10-tetracarboxylic dianhydride (PTCDA), are applied as cathode materials in lithium-organic batteries.[28,29] AQ (yellow colour, Fig. 3a) and PTCDA (red colour, Fig. 3b), both of which are rodlike, possess 2 and 4 carbonyl groups in each molecule, respectively (insets in Fig. 3c and d). The reduction/oxidation potentials of the two organic cathodes are revealed by their cyclic voltammetry (CV) curves. The CV curve for the AQ electrode presents a reduction peak at ~2.2 V and an oxidation peak at ~2.4 V[30] (Fig. 3c). For the CV curve of the PTCDA electrode, there are two reduction peaks (at 2.4 V and 2.5 V) and one oxidation peak (at 2.7 V) (Fig. 3d).

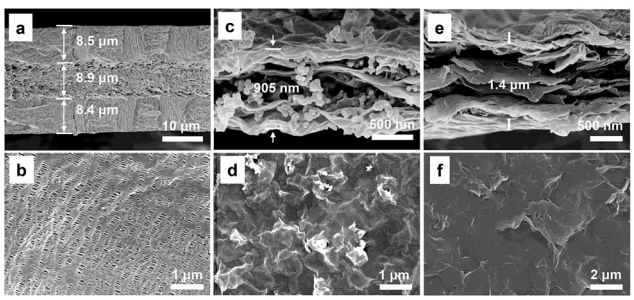

Fig. 2 SEM images of the pristine and the coated separators. (a) Cross-sectional and (b) top-view SEM image of the pristine Celgard separator with the triple-layered structure of PP/PE/PP; (c) cross-sectional and (d) top-view SEM images of the GO/SP bicomponent layer; (e) cross-sectional and (f) top-view SEM images of the GO/G bicomponent layer.

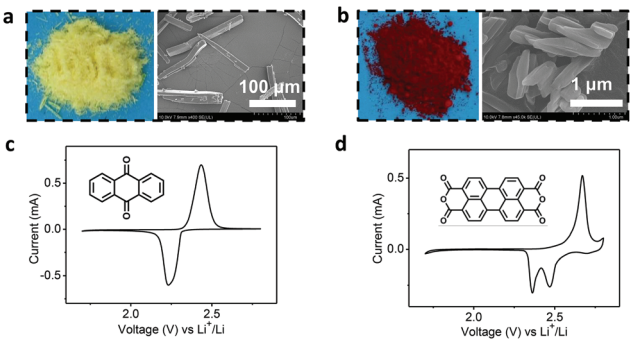

Fig. 3 Digital photograph (left) and SEM image (right) of the organic molecules of (a) AQ and (b) PTCDA. Retention of the OCV of (c) the AQ electrode and (d) the PTCDA electrode with the pristine separator and the coated separators with the dual components GO/SP and GO/G. Insets: The molecular structures of (c) AQ and (d) PTCDA.

The electrochemical reaction mechanisms of the two organic molecules are expressed in Fig. 4a and b. Between the voltage window of 1.7 V and 3.5 V (*versus* Li^+/Li), both AQ and PTCDA bear a two-electron reversible reaction process, which make their theoretical capacities 257 and 132 mA h g^{-1}, respectively. The other two carbonyl groups in the PTCDA molecule can be further reduced only at voltages lower than 1.3 V (*versus* Li^+/Li); so they do not contribute capacity herein.[31]

AQ and PTCDA, as well as their discharged intermediates and products, are easily solvable in the liquid electrolyte. Normally, smaller molecules tend to dissolve more easily. Because of this tendency, a quasi-solid state electrolyte[32] and a solid-state electrolyte[33] can be effective approaches for improving the performance of small organic molecules, as well as polymerization[31,34–36] or confinement[37–39] of the organic molecules. In this work, the ion selective separator approach is applied. The size of the AQ molecule is smaller than that of the PTCDA molecule; hence AQ is utilized as an example for demonstrating the dissolution of the electroactive organic species and the ion selective separator addressing this problem.

The yellow colour of a concentrated solution of AQ in the electrolyte proves its dissolution. Besides, after disassembling a coin cell with a pristine separator and an AQ cathode, it was seen that both the separator and the lithium anode were contaminated by AQ-related organic species. In contrast, the lithium anode coupled with GO/SP-P was uncontaminated. The inhibited contamination of the lithium anode with GO/SP-P suggests that the GO/SP bicomponent layer on the Celgard substrate accommodates and blocks the dissolved AQ-related organic species.

Furthermore, the ion selectivity of the bicomponent layer of GO/SP was demonstrated by a visual diffusion experiment on a H-type glass cell. It can be seen that, in the case of pristine P after 24 h, the organic molecules and anions dissolved on the left side diffused to the right side (Fig. 5a and b). In contrast, with the GO/SP-P separator, the active materials were blocked, and the right side remained colourless after the same length of time (Fig. 5c and d). The cation permselectivity of the GO/SP layer originates from the GO sub-layer, which possesses abundant negatively charged nanochannels between the reconstructed GO sheets. The reconstructed GO sheets are the basic configuration of the bicomponent layer and are needed to form a dependent membrane and accommodate the SP particles. The GO sheets overlap with each other and produce negatively charged nanochannels with a dimension comparable to the Debye length, thereby regulating ion transport by allowing the migration of lithium ions and rejecting the electroactive organic anions.[25,27]

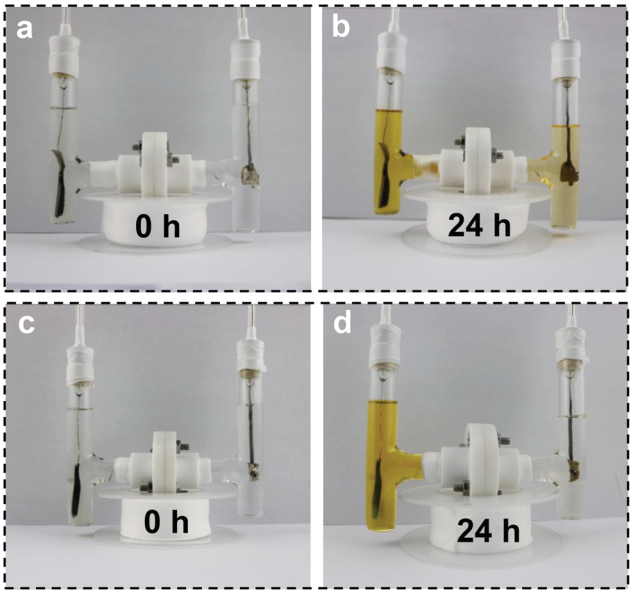

Fig. 5 Visual images of a diffusion cell with (a, b) a pristine Celgard separator and (c, d) a GO/SP-P separator. The working electrode is AQ and the reference electrode is lithium foil. The applied potential is 2.2 V with duration of 24 h.

The OCV of the AQ and the PTCDA electrodes with the coated separators remains significantly more stable than those with pristine P, as shown in Fig. 6. The OCV of the AQ (Fig. 6a) and the PTCDA (Fig. 6b) electrodes with pristine P dropped to approximately 1.7 V after resting for 31 and 22 h, respectively, far below the discharge voltage plateaus, while those with the coated separators were retained. When the battery with pristine P was rested, the continuous dissolution of organic molecules inevitably resulted in the OCV drop, which seriously shortened the shelf-life of the batteries. In contrast, for the bicomponent-layer-coated separators, the coating layer of GO/

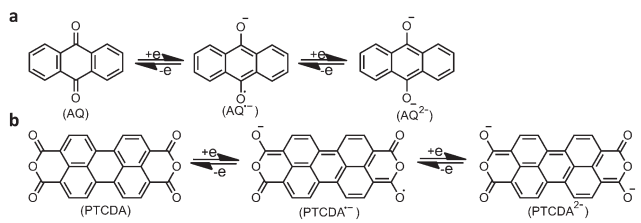

Fig. 4 An electrochemical redox mechanism for the two molecules: AQ and PTCDA.

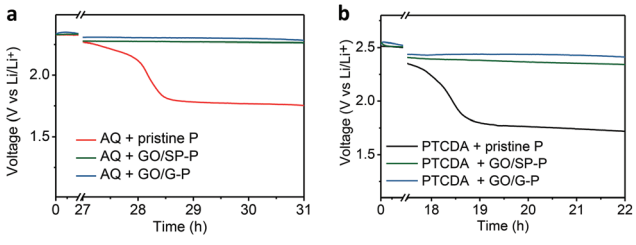

Fig. 6 Retention of the OCV of (a) the AQ electrode and (b) the PTCDA electrode with the pristine separator and the coated separators with the dual components GO/SP and GO/G. Insets: The molecular structures of (c) AQ and (d) PTCDA.

SP or GO/G functions as a buffering zone to mitigate the migration of the soluble organic materials, which greatly stabilizes the OCV and alleviates the self-discharge of the electrodes.

The GO/SP or GO/G bicomponent layer improves not only the OCV stability of the AQ or PTCDA electrodes, but also the capacity and the cycling stability (Fig. 7). At 100 mA g^{-1}, the AQ cathode with GO/SP-P or GO/G-P shows higher capacity at the initial cycle, and GO/SP-P particularly exhibits a significantly improved initial specific capacity of 233.3 mA h g^{-1}, compared to 201.9 mA h g^{-1} for pristine P (Fig. 7a). After 150 cycles, both the coated separators show similar capacities of around 100 mA h g^{-1}, almost double the 50 mA h g^{-1} specific capacity for the pristine separator. Fig. 7b shows the charge/discharge voltage profiles for the cells with GO/SP-P and pristine P after 100 cycles. The discharge capacity for the coated separator is much higher than that for the pristine separator (104 *vs.* 64 mA h g^{-1}). As can be seen from the results, for the AQ electrode, both GO/SP-P and GO/G-P have similar effects on battery performance in terms of capacity and cycling stability.

The effects of the coated separators were also demonstrated by the PTCDA cathode. GO/SP-P and GO/G-P show greatly improved cycling stability compared to pristine P (Fig. 7c). In particular, the specific capacity at the 200th cycle for GO/SP-P is 104 mA h g^{-1}, almost triple the 36 mA h g^{-1} specific capacity for the cell with pristine P. Moreover, the CE is significantly improved. For the cell with pristine P, the CE gradually drops to around 90% and remains lower than 90% for the rest of the charge/discharge cycling. In contrast, both GO/G-P and GO/SP-P present CE above 99.5%. The charge/discharge voltage profiles at the 200th cycle for the cells with GO/G-P and pristine P are presented in Fig. 7d. The results indicate significantly improved discharge capacity and CE (78.0 *vs.* 36.3 mA h g^{-1} and 99.7% *vs.* 75.6%). The results of the cells with the PTCDA cathode indicate that both the coated separators, GO/SP-P and GO/G-P, exhibit significant positive effects on battery performance in terms of capacity, CE, and cycling stability. GO/SP-P, in particular, shows the best behaviour among the three separators.

The significantly improved battery performance from several important aspects such as cycling stability and self-discharge property is ascribed to the thin coating layer with dual components of GO and SP (or G). The normalized capacity contributions of the two bicomponent layers are insignificant (3 mA h g^{-1} for GO/SP and 7 mA h g^{-1} for GO/G), indicating that most of the enhanced capacity originates from the improved utilization of the electroactive organic materials due to the separator functionalization. In a bicomponent layer, the GO sub-layer is composed of reconstructed GO nanosheets, which form nanochannels with negative charge carried by the functional groups of carboxylic acid and phenolic hydroxyl. The dimension of the negatively charged nanochannels (around 1 nm) is comparable to the Debye length, so that they reject the transport of anions but allow the fast migration of lithium ions.[40] Because of this feature, the electroactive organic anions are retained on the cathode side of the lithium-organic cell. Moreover, the other sub-layer composed of SP or G acts as an upper current collector, reactivating the inactive electroactive organic molecules/anions at the cathode/separator interface. Both the GO and the SP (or G) components synergistically increase the utilization of the active material and hence improve the capacity, the cycling stability, the CE, and the anti-self-discharge capability of the cell.

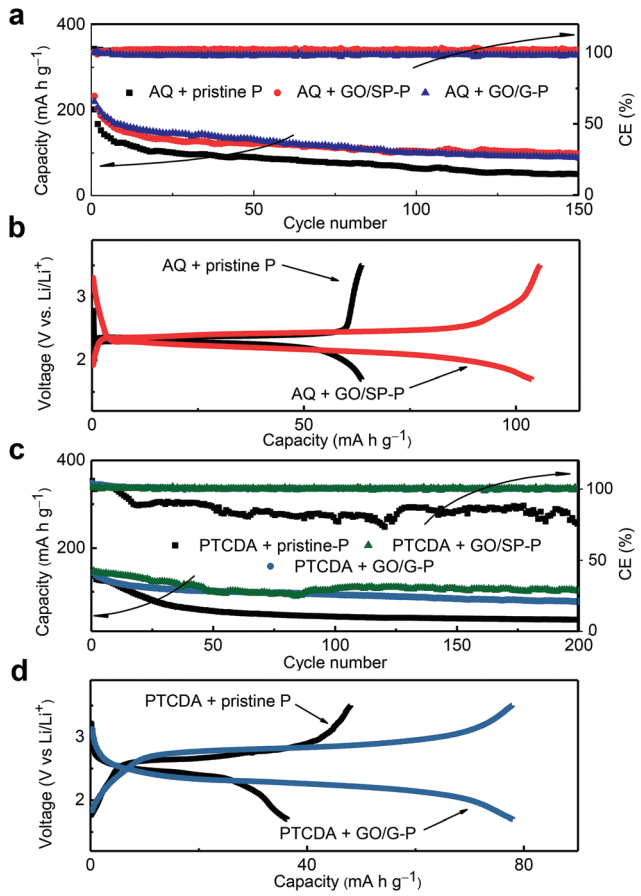

Fig. 7 Battery performances of AQ and PTCDA electrodes with different separators. (a) Cycling behavior of the AQ electrode with pristine P, GO/SP-P and GO/G-P. (b) Charge/discharge voltage profiles of the AQ electrode with pristine P and the GO/SP-P separators at the 100th cycle. (c) Cycling behavior and coulombic efficiency of the PTCDA electrode with pristine P, GO/SP-P and GO/G-P. (d) Charge/discharge voltage profiles of the PTCDA electrode with pristine P and the GO/G-P separators at the 200th cycle.

Conclusions

In summary, a new strategy of bicomponent coating (thickness of approximately 1 μm and areal density of around 0.1 mg cm^{-2}) on the Celgard separator has been applied to improve the electrochemical performances of lithium-organic batteries. In the coating layer, GO sheets are reconstructed and form numerous negatively charged nanochannels to selectively allow the transport of lithium ions; meanwhile, Super P (or

graphene) acts as an upper current collector to improve the utilization of the active materials. Two carbonyl organic molecules, AQ and PTCDA, are applied as examples of the cathode materials. It has been demonstrated that the OCV stability has been enhanced, and the specific capacity and the cycle life improved, compared to the cells with the pristine Celgard separator. For instance, with either GO/SP-P or GO/G-P, the AQ cathode shows a capacity of 100 mA g^{-1}, double the capacity (50 mA h g^{-1}) of the cell with pristine P after 150 cycles at 100 mA g^{-1}. Besides, the PTCDA cathode with GO/SP-P has almost triple the specific capacity of the cell with pristine P (104 *vs.* 36 mA h g^{-1}) after 200 cycles. The advanced performance of these lithium-organic batteries is attributed to the synergetic functions of the dual components in the coating layer: the rejection of the electroactive organic anions by the negatively charged nanochannels between the reconstructed GO sheets and the reactivation of the dissolved electroactive organic species by Super P (or graphene) as an upper current collector. This novel strategy of separator coating with a thin bicomponent layer is expected to be extended to other similar electrochemical energy storage.

Conflicts of interest

There are no conflicts of interest to declare.

Acknowledgements

We acknowledge the financial support by the National Science Foundation of China (21504097), the Key Research Program of the Chinese Academy of Sciences (KJZD-EW-M03), the Frontier Science Key Projects of CAS (QYZDY-SSW-SLH014), the Discovery Project (DP160102627) and the Linkage Project (LP120200432). All authors have given approval to the final version of the manuscript.

References

1 P. Arora and Z. M. Zhang, *Chem. Rev.*, 2004, **104**, 4419.
2 S. S. Zhang, *J. Power Sources*, 2007, **164**, 351.
3 M. Armand and J. M. Tarascon, *Nature*, 2008, **451**, 652.
4 F. Y. Cheng, J. Liang, Z. L. Tao and J. Chen, *Adv. Mater.*, 2011, **23**, 1695.
5 H. Lee, M. Yanilmaz, O. Toprakci, K. Fu and X. W. Zhang, *Energy Environ. Sci.*, 2014, **7**, 3857.
6 Y. Pan, S. Chou, H. K. Liu and S. X. Dou, *Natl. Sci. Rev.*, 2017, **4**, 917.
7 J.-A. Choi, S. H. Kim and D.-W. Kim, *J. Power Sources*, 2010, **195**, 6192.
8 Z. Z. Yuan, Y. Q. Duan, H. Z. Zhang, X. F. Li, H. M. Zhang and I. Vankelecom, *Energy Environ. Sci.*, 2016, **9**, 441.
9 T. Ma, Z. Pan, L. Miao, C. Chen, M. Han, Z. Shang and J. Chen, *Angew. Chem., Int. Ed.*, 2018, **57**, 3158.
10 J. X. Leong, W. R. W. Daud, M. Ghasemi, K. Ben Liew and M. Ismail, *Renewable Sustainable Energy Rev.*, 2013, **28**, 575.
11 Z. Q. Jin, K. Xie, X. B. Hong, Z. Q. Hu and X. Liu, *J. Power Sources*, 2012, **218**, 163.
12 J.-Q. Huang, Q. Zhang, H.-J. Peng, X.-Y. Liu, W.-Z. Qian and F. Wei, *Energy Environ. Sci.*, 2014, **7**, 347.
13 J. Q. Huang, T. Z. Zhuang, Q. Zhang, H. J. Peng, C. M. Chen and F. Wei, *ACS Nano*, 2015, **9**, 3002–3011.
14 T. Z. Zhuang, J. Q. Huang, H. J. Peng, L. Y. He, X. B. Cheng, C. M. Chen and Q. Zhang, *Small*, 2016, **12**, 381–389.
15 P. He, T. Zhang, J. Jiang and H. S. Zhou, *J. Phys. Chem. Lett.*, 2016, **7**, 1267.
16 B. Häupler, A. Wild and U. S. Schubert, *Adv. Energy Mater.*, 2015, 1402034.
17 Y. L. Liang, Z. L. Tao and J. Chen, *Adv. Energy Mater.*, 2012, **2**, 742.
18 X. Li, A. Lushington, Q. Sun, W. Xiao, J. Liu, B. Wang, Y. Ye, K. Nie, Y. Hu, Q. Xiao, R. Li, J. Guo, T.-K. Sham and X. Sun, *Nano Lett.*, 2016, **16**, 3545.
19 A. Manthiram, Y. Fu, S.-H. Chung, C. Zu and Y.-S. Su, *Chem. Rev.*, 2014, **114**, 11751.
20 Y. Pan, S.-L. Chou, H.-K. Liu and S.-X. Dou, *RSC Adv.*, 2016, **6**, 34131.
21 H. L. Pan, X. L. Wei, W. A. Henderson, Y. Y. Shao, J. Z. Chen, P. Bhattacharya, J. Xiao and J. Liu, *Adv. Energy Mater.*, 2015, 1500113.
22 Z. Song, Y. Qian, M. Otani and H. Zhou, *Adv. Energy Mater.*, 2016, 1501780.
23 C. X. Zu, Y. S. Su, Y. Z. Fu and A. Manthiram, *Phys. Chem. Chem. Phys.*, 2013, **15**, 2291.
24 D. Li, M. B. Muller, S. Gilje, R. B. Kaner and G. G. Wallace, *Nat. Nanotechnol.*, 2008, **3**, 101.
25 K. Raidongia and J. Huang, *J. Am. Chem. Soc.*, 2012, **134**, 16528.
26 X. Zhu, Y. Zhou, H. Junran, B. Bao, X. Bian, X. Jiang, J. Pang, H. Zhang, Z. Jiang and L. Jiang, *ACS Nano*, 2017, **11**, 10816.
27 Y. Pan, Y. Zhou, Q. Zhao, Y. Dou, S. Chou, F. Cheng, J. Chen, H. K. Liu, L. Jiang and S. X. Dou, *Nano Energy*, 2017, **33**, 205.
28 Z. Song and H. Zhou, *Energy Environ. Sci.*, 2013, **6**, 2280.
29 K. C. Kim, T. Liu, S. W. Lee and S. S. Jang, *J. Am. Chem. Soc.*, 2016, **138**, 2374.
30 A. J. Wain, G. G. Wildgoose, C. G. R. Heald, L. Jiang, T. G. J. Jones and R. G. Compton, *J. Phys. Chem. B*, 2005, **109**, 3971.
31 X. Han, C. Chang, L. Yuan, T. Sun and J. Sun, *Adv. Mater.*, 2007, **19**, 1616.
32 W. Huang, Z. Zhu, L. Wang, S. Wang, H. Li, Z. Tao, J. Shi, L. Guan and J. Chen, *Angew. Chem., Int. Ed.*, 2013, **52**, 9162.
33 Z. Zhu, M. Hong, D. Guo, J. Shi, Z. Tao and J. Chen, *J. Am. Chem. Soc.*, 2014, **136**, 16461.
34 T. Le Gall, K. H. Reiman, M. C. Grossel and J. R. Owen, *J. Power Sources*, 2003, **119**, 316.
35 Z. Song, H. Zhan and Y. Zhou, *Chem. Commun.*, 2009, 448.

36 M. Miroshnikov, K. P. Divya, G. Babu, A. Meiyazhagan, L. M. Reddy Arava, P. M. Ajayan and G. John, *J. Mater. Chem. A*, 2016, **4**, 12370.
37 S. Zheng, J. Hu and W. Huang, *Inorg. Chem. Front.*, 2017, **4**, 1806.
38 L. Zhao, W. Wang, A. Wang, Z. Yu, S. Chen and Y. Yang, *J. Electrochem. Soc.*, 2011, **158**, 991.
39 H. Li, W. Duan, Q. Zhao, F. Cheng, J. Liang and J. Chen, *Inorg. Chem. Front.*, 2014, **1**, 193.
40 H. Daiguji, *Chem. Soc. Rev.*, 2010, **39**, 901.